Journal of Materials Chemistry A

PAPER

View Article Online
View Journal | View Issue

Cite this: J. Mater. Chem. A, 2017, 5, 2981

Multifunctional porous organic polymers embedded with magnetic nanoparticles†

Shanlin Qiao,[ab] Wei Huang,[c] Ting Wang,[c] Bin Du,*[a] Xiangning Chen,[a] Abdul Hameed[d] and Renqiang Yang*[c]

Received 16th November 2016
Accepted 19th December 2016

DOI: 10.1039/c6ta09917c

www.rsc.org/MaterialsA

Multifunctional hybrid polycarbazoles were prepared with a novel core–spacer–shell structure. Magnetism, a conjugated system and an ultramicroporous structure are combined in one bulk material. SEM and TEM images show the obvious core@shell structure in the nano-region. Nitrogen gas sorption, magnetic and surface wettability analyses indicate the multifunctionality of the obtained materials. Their high efficiency dynamic adsorption (water treatment) and static separation (CH_4/CO_2 gas selectivity) allow these novel materials to be employed as facile tools for environmental treatment and in energy storage fields.

Introduction

Recently, extensive research has been undertaken to study novel and multifunctional porous materials, which have shown great promise for environmental treatment and energy related applications. Porous organic polymers (POPs) especially conjugated microporous polymers (CMPs) have attracted great interest as a new class of advanced materials due to their unique structures combining extended p-conjugation with microporous polymers.[1] CMPs have advantages like low mass density, high chemical and thermal stability, tunable pore size and large surface areas which make them highly competitive with other porous materials. CMPs have demonstrated great potential for water system treatment, pollutant adsorption and separation,[2] gas storage,[3] supercapacitive energy storage,[4] heterogeneous catalysis,[5] and chemosensing.[6]

How to design CMP materials with multiple functions and thereby expand their applications is a meaningful and imperative subject. (1) Magnetic carrier technology (MCT) has been an important tool in biological and environmental 珋elds since it was reported.[7] The prominent advantage of MCT is that magnetic materials can automatically assemble under an external magnetic 珋eld. Therefore, the combination of MCT and ultramicropores in one structure to form multifunctional materials is signi珋cative. (2) Core–shell structures are of more interest in nanoscience and the colloid 珋eld,[8] and can provide a facile way to fabricate hybrid materials. Fe_3O_4 magnetic nanoparticles owing to their superparamagnetism, large saturation magnetization, high magnetic susceptibility and low toxicity have been used in the magnetic 珋eld.[9] However, Fe_3O_4 nanoparticles (Fe_3O_4 NPs) suffer from some inherent limitations such as easy aggregation, oxidation and variable magnetic properties in complex systems.[10] The above limitations and the structure of cellulose[11] and chitosan[12] inspire us to explore a new extraction method by coating magnetic NPs with microporous polymers to design a hydrophobic lightweight protective shell. Based on the above background, to prepare a hybrid material (core@shell) combined with magnetism, p-conjugation and microporosity would be interesting. The shell formed by rigid highly crosslinked CMP networks could prevent the core Fe_3O_4 NPs from aggregation and oxidation effectively; at the same time the Fe_3O_4 NP core was anticipated to endow the microporous polymer with magnetic properties. Tan and Gao reported the hypercrosslinking of precursors to produce magnetic microporous polymer nanoparticles (MMPNs) and Fe_3O_4/SiO_2/P(MAA-co-VBC-co-DVB), respectively.[13] Zhu used a microwave-enhanced high-temperature ionothermal method to prepare a magnetic porous carbonaceous polymeric material for organic dye separation.[14] In this work, we designed and prepared magnetic microporous materials with a miraculous core@shell structure and they have a good adsorption ability. The $CaCO_3$ template method is an effective way to enlarge the pore volume of materials,[15] in which Fe_3O_4 NPs are used as a core and coated with a $CaCO_3$ template, and then different thickness CMP shells are formed by further polymerization of poly(N-vinylcarbazole) (PVK) to form a polycarbazole conjugated shell. More reports have shown that conjugated polycarbazoles

[a]Beijing Key Laboratory of Agricultural Product Detection and Control of Spoilage Organisms and Pesticide Residue, Faculty of Food Science and Engineering, Beijing University of Agriculture, Beijing 102206, China. E-mail: bindu80@bua.edu.cn
[b]Institute of Chemical Industry and Pharmaceutical Engineering, Hebei University of Science and Technology, Shijiazhuang 050000, China
[c]CAS Key Laboratory of Bio-based Materials, Qingdao Institute of Bioenergy and Bioprocess Technology, Chinese Academy of Sciences, Qingdao 266101, China. E-mail: yangrq@qibebt.ac.cn
[d]CAS Key Laboratory of Standardization and Measurement for Nanotechnology, CAS Center for Excellence in Nanoscience, National Center for Nanoscience and Technology, Beijing 100190, P. R. China

† Electronic supplementary information (ESI) available: FT-IR and NMR spectra, TGA, UV-vis absorption spectra, XRD patterns, particle size distribution, and SEM and TEM images. See DOI: 10.1039/c6ta09917c

are a potential candidate in the organic porous 珔eld.[16] The detailed illustration of the preparation procedure is shown in Scheme 1. $CaCO_3$ is of low cost and easily etched by acid pickling. A泹er removing the $CaCO_3$ template with acetic acid, abundant hollow cavities were shaped between the Fe_3O_4 NP core and CMP shell which can generate hierarchical porosities and enlarge the total pore volume. Varying the content of Fe_3O_4 NPs can tune the magnetic strength and the pore parameters of the hybrid materials. The easily fabricated hierarchical material would maintain the advantages of both components and promote the actual utilization performance.

Experimental

Materials

Toluene, tetrahydrofuran (THF) and chloroform were puri珔ed by distillation prior to use. 2,2^0-Azobis-isobutyronitrile (AIBN) and N-vinyl carbazole (VCz) were purchased from J&K and anhydrous ferric chloride was obtained from Aldrich and used as received. Ferric chloride hexahydrate ($FeCl_3$\$$6H_2O$), ferrous chloride tetrahydrate ($FeCl_2$\$$4H_2O$), sodium hydroxide (NaOH), anhydrous sodium carbonate (Na_2CO_3), calcium chloride ($CaCl_2$), and acetic acid (HAc) were all obtained from J&K or Aldrich. Ultrapure water was prepared in the lab using a Milli-Q SP reagent water system (Millipore, Bedford, MA, USA).

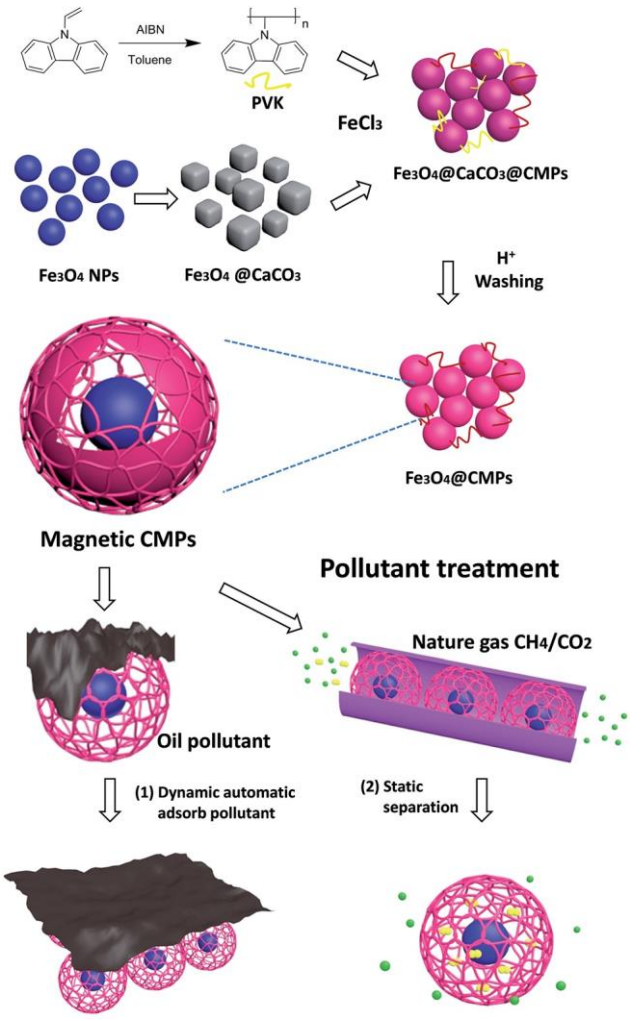

Scheme 1 Synthetic route for Fe_3O_4@CMP preparation and diagram for treatment of pollutants.

1. Fe_3O_4 nanoparticles. Fe_3O_4 nanoparticles were prepared by a chemical co-precipitation method as reported in the literature.[10] 5.2 g of $FeCl_3$\$$6H_2O$, 2.0 g of $FeCl_2$\$$4H_2O$ and 0.85 mL of HCl (12 mol L^{-1}) were dissolved in 25 mL of deionized water (degassed with nitrogen gas before using) to prepare a stock solution. 250 mL of 1.5 mol L^{-1} NaOH solution was heated to 80 °C in a beaker. The stock solution was added dropwise under nitrogen gas protection and vigorous stirring using a non-magnetic stirrer. A泹er the reaction completion, the obtained Fe_3O_4 NP precipitate was separated from the reaction medium by 珔ltration, and dried under vacuum at room temperature a泹er washing four times with 200 mL of deionized water.

2. Fe_3O_4@$CaCO_3$. Fe_3O_4@$CaCO_3$ composites were prepared by a previously reported chemical co-precipitation method.[2] To prepare the Fe_3O_4@$CaCO_3$ composites, calcium chloride (0.6 M) was dissolved in 50 mL of the as-prepared Fe_3O_4 suspension under vigorous stirring. Then equal volumes of Na_2CO_3 solutions (with equal salt concentrations) were rapidly added, followed by stirring at room temperature for 4 h.[3] The solid was separated and washed with ultrapure water three times, and 珔nally dried under vacuum for 12 h.

3. Poly(N-vinylcarbazole) (PVK). A typical procedure to prepare PVK is as follows: VCz (1.5 g, 7.75 mmol) and AIBN (55.5 mg, 0.39 mmol) were dissolved in dry toluene and the mixture was put into a two-neck round bottom 瑢ask. The mixture was heated at an operational temperature of 70 °C and stirred for 6 h under a nitrogen atmosphere. The solid was separated by 珔ltration and washed three times with methanol and dried under vacuum at room temperature for 48 h to get a white solid (1.2 g, 80% yield).

4. Fe_3O_4@CMPs (Fe_3O_4 : CMPs ¼ 10%, 20%, 30%, 40%) and pure CMPs. To synthesize Fe_3O_4@CMP composites with different composition ratios, Fe_3O_4@$CaCO_3$ particles (20, 40, 60, and 80 mg) and PVK (200 mg) were dispersed in 30 mL anhydrous chloroform and stirred for 0.5 h at 0 °C. A suspension of ferric chloride (1.38 g, 8.28 mmol) in 20 mL of anhydrous chloroform was transferred dropwise to the above mixture under nitrogen protection at room temperature. The solution mixture was mechanically stirred for 24 h at room temperature under nitrogen protection, and then 100 mL of methanol was added to the mixture. The resulting precipitate was collected by 珔ltration and washed with methanol and ultrapure water. Then, the materials were dispersed in 120 mL acetic acid solution (HAc : methanol : H_2O ¼ 1 : 1 : 10) for 24 h and collected by 珔ltration. The obtained material was extracted in a Soxhlet extractor with methanol for 24 h, and then with THF for another 24 h, a泹er which the desired polymer was collected as a grey white solid and dried in a vacuum oven at 80 °C overnight (204 mg (92%), 221 mg (92%), 239 mg (92%), and 253 mg (90%)). Pure CMPs without Fe_3O_4 NPs were also synthesized through the same procedure as that given in ref. 17.

Characterization

The structures of PVK and pure CMPs were confirmed by ^{13}C CP/MAS solid-state NMR spectroscopy on a Bruker Avance III model 400 MHz NMR spectrometer at a MAS rate of 5 kHz. All the materials were also characterized by ATR-IR spectra which were collected in attenuated total reflection (ATR) mode on a Thermo Nicolet 6700 FT-IR Spectrometer. Thermogravimetric analysis (TGA) was carried out using an SDT Q600 V20.9 Build 20 with a temperature ramp of 10 °C min^{-1} from 20 to 800 °C. The magnetic properties were analysed on a Squid VSM (Quantum Design). Scanning electron microscopy (SEM) was performed using a Nova™ NanoSEM 430 (FEI Company) with acceleration voltage 5.0 kV and working distance 6.9 mm or 7.0 mm. Transmission electron microscopy (TEM) was performed using a Hitachi H-7650. The particle size distribution was measured on a Laser Particles Distribution Instrument (LPDI) Malvern Zetasizer Nano S90, and four hybrid polymers were dispersed in ethanol under ultrasound conditions for 5 h. The residual Ca content was determined using inductively coupled plasma mass spectrometry (ICP-MS, Agilent 7500a) after the polymers were fully dispersed in concentrated nitric acid. All the samples were tested on an Autosorb-iQ-MP-VP volumetric adsorption analyser with the same degassing procedure. And the polymers were degassed at 120 °C for 10 h under vacuum before analysis to remove residual moisture and other trapped gases. The BET surface areas and pore size distributions were measured by nitrogen adsorption–desorption at 77 K in a liquid nitrogen bath. CO_2 and CH_4 uptake capacities were measured at 273 K up to 1.0 bar. H_2 adsorptions were determined at 77 K from zero to 1.0 bar.

Results and discussion

The molecular structure of CMPs was confirmed by ATR-IR and ^{13}C CP/MAS spectra. Four hybrid materials have been prepared with an Fe_3O_4 weight ratio from 10% to 40% (the material named 30% Fe_3O_4@CMPs represents that the mass of Fe_3O_4 compared to that of the CMPs is 30%). The ATR-IR spectra of Fe_3O_4 NPs, Fe_3O_4@$CaCO_3$, and Fe_3O_4@CMPs are shown in Fig. S1.† The ATR-IR spectra of the four Fe_3O_4@CMP products were exactly similar and the peaks are characteristic of PVK as previously reported.[18] The NMR spectra of PVK and the pure CMP shell without magnetic Fe_3O_4 NPs have been measured to confirm the molecular structure of CMPs (Fig. S2†). The broad peaks at 35, 50, 110, 120, 124 and 139 ppm are typical characteristic peaks of N-vinyl carbazole and demonstrate the successful polymerization of N-vinyl carbazole. The hybrid polycarbazoles exhibit excellent heat resistance with decomposition temperatures (T_d 10%) up to *ca.* 444, 434, 441 and 436 °C for 10, 20, 30 and 40 wt% Fe_3O_4@CMPs, respectively (Fig. S3†). As the main UV-vis absorption bands occur at 261, 295, 331 and 344 nm for pure PVK,[19] the broad absorption bands from 200 to 400 nm of the UV-vis spectra in Fig. S4† confirm the structure of poly(N-vinylcarbazole). The maximum absorption peak of Fe_3O_4 which should be around 300 nm is overlapped with the bands of poly(N-vinylcarbazole). To investigate the morphologies, powder X-ray diffraction (P-XRD, Fig. S5a–d†) was used and the results show the Fe_3O_4@CMPs without any crystalline phase, assigned to an amorphous aggregation. The size distributions of the hybrid materials which were measured using the LPDI show that the polymers have a uniform particle dimension and the particle sizes have little relationship with the concentration of Fe_3O_4@$CaCO_3$ NPs added. The domain particle dimension of the 10% Fe_3O_4@CMPs is around 164 nm, 20% Fe_3O_4@CMPs is 167 nm, 30% Fe_3O_4@CMPs is 142 nm and 40% Fe_3O_4@CMPs is 121 nm (Fig. S6†).

The SEM images of the Fe_3O_4 NPs, Fe_3O_4@$CaCO_3$, 30% Fe_3O_4@CMPs, and CMP are shown in Fig. 1a–d and S7.† The Fe_3O_4 NPs have a relatively non-uniform hard surface aggregated by plenty of Fe_3O_4 nanoparticles. The Fe_3O_4@$CaCO_3$ particles possess a clear homogeneous and cubic morphology which is remarkably different from that of the naked Fe_3O_4 NPs caused by the coating of $CaCO_3$. This means that the Fe_3O_4 NPs are covered by $CaCO_3$ particles successfully. The prepared hybrid materials have similar aggregation morphologies consisting of relatively uniform spheres. After being etched with acetic acid, the cubic particles disappeared and were replaced by the spherical particles. The TEM images show the inside of the Fe_3O_4@CMP particles. The core (the shadow region) was embedded in the CMP shell (the outside pale region) heterogeneously as the obvious core@shell structure, and the size dimension of the Fe_3O_4 NP core ranges from 30 to 80 nm (Fig. 1e, more images are shown in Fig. S8†). After washing with acetic acid solution, some spheroidal holes (the white

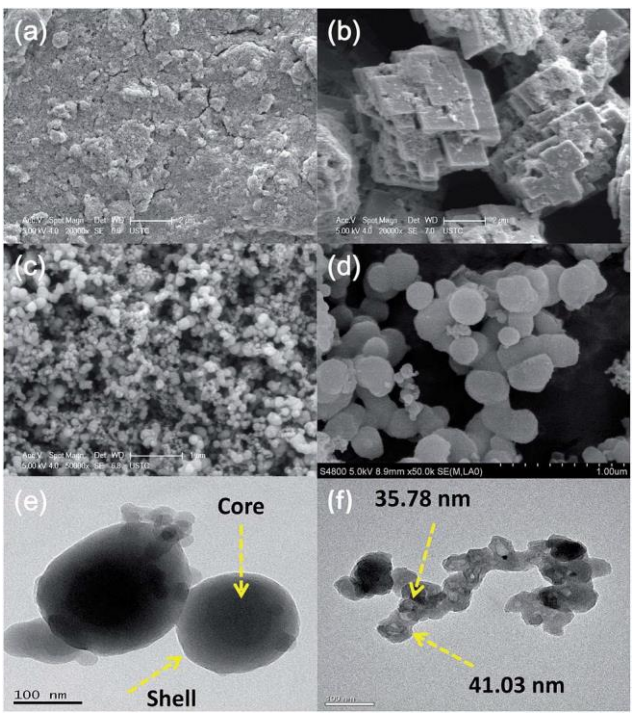

Fig. 1 SEM images of the (a) Fe_3O_4 NPs, (b) Fe_3O_4@$CaCO_3$, (c) 30% Fe_3O_4@CMPs and (d) polycarbazole network. TEM images of (e) 30% Fe_3O_4@CMPs, (f) Fe_3O_4 NP cores and etched $CaCO_3$ holes; the yellow arrows indicate the core and shell.

transparent region) were formed in the bulk polymers by H^+ etching the $CaCO_3$ (Fig. 1f, more images are shown in Fig. S9†), and the size dimension of the holes ranges from 20 to 100 nm, indicating that etching is an effective way to enlarge the pore volume of materials. The TEM images provide strong evidence for the success of this template method, and the magnetic Fe_3O_4 cores are totally covered by the highly crosslinked microporous shells which is beneficial to protect them from aggregation and oxidation effectively.

The $CaCO_3$ template method could enhance the pore volume, but the removal of the residual template from microporous polymers is hard work. The content of the remaining Ca element was determined by ICP-MS, which was 2.543 mg g^{-1} for 10% Fe_3O_4@CMPs, 1.347 mg g^{-1} for 20% Fe_3O_4@CMPs, 9.034 mg g^{-1} for 30% Fe_3O_4@CMPs and 28.33 mg g^{-1} for 40% Fe_3O_4@CMPs.

Nitrogen gas adsorption analysis

The porous structures of the hybrid materials Fe_3O_4@CMPs were investigated using nitrogen isotherms at 77 K shown in Fig. 2a.[20] To deeply understand the porous structure of the Fe_3O_4@CMPs, the nitrogen isotherm of the naked Fe_3O_4 NPs was also measured. It can be seen that the naked Fe_3O_4 NPs give rise to a type V nitrogen sorption isotherm with N_2 hysteresis loops according to the IUPAC classification (the pore size distributions are shown in Fig. S10† calculated by nonlocal density functional theory (NLDFT)).[21] The prepared Fe_3O_4@CMPs exhibit similar adsorption–desorption isotherms, which are combinations of type I and II nitrogen sorption isotherms.[20] The predominant microporous structures were confirmed by the isotherms in which a high uptake was obtained at relatively low pressures (P/P_0 ¼ 0–0.01). The gradual increase in adsorption branches under moderate pressures and a sharp gas uptake at high pressures above 0.9 (P/P_0) may be due to some mesoporosity and interparticle voids.[22]. The detailed porous parameters of the prepared materials are shown in Table S1.† The BET surface areas of the Fe_3O_4@CMPs with different hybrid ratios decrease with the addition of Fe_3O_4 as the values are 735, 680, 636, and 518 $m^2 g^{-1}$ for 10% Fe_3O_4@CMPs to 40% Fe_3O_4@CMPs, respectively. The BET surface areas of the Fe_3O_4@CMPs are much higher than those of the naked Fe_3O_4 NPs, but lower than those of CMPs without a magnetic core. This can be explained in the way that the low porosity magnetic core results in decreasing of the BET surface areas due to the weight contribution. Although the composite materials have lower surface areas, the total pore volumes are higher or competitive compared to those of pure CMPs (Fig. 2b and Table S1†). Thus, there should be some spacers between the Fe_3O_4 core and CMP shell after the etching of the $CaCO_3$ layer. It is worth mentioning that the materials prepared by the template method have a relatively large pore volume as hollow cavities exist between the core and shell. The narrow pore size of less than 2 nm which should belong to the shell structure represents a typical microporous/mesoporous distribution of the conjugated organic networks (Fig. S10†). The similar domain sizes of the Fe_3O_4@CMPs with different core ratios indicate that the microporous size distributions of the core@shell structure mainly depend on the shell network and have almost no relation to the magnetic core. So the shell structures may be the main region for small molecular separation, and the nature of the conjugated shell networks would play key role for the hybrid materials.

Magnetic, wettability and pollutant treatment (water/gas system)

The hysteresis loops of the Fe_3O_4 NPs, Fe_3O_4@$CaCO_3$, and Fe_3O_4@CMPs were measured at room temperature (Fig. 3a and S11†). It is clear that the materials exhibit typical superparamagnetic behaviour as there is no hysteresis, remanence or coercivity. It is obvious that the maximal saturation magnetization value of the hybrid core@shell structure is increased as the ratio of the Fe_3O_4 NPs is increased, with 40% Fe_3O_4@CMPs reaching 2.99 emu g^{-1}, indicating that the core weight contribution is crucial for the magnetic intensity. In particular, 10% and 20% Fe_3O_4@CMPs can hardly stick to a magnet due to their weak magnetisms. As to 30% and 40% Fe_3O_4@CMPs the maximal saturation magnetizations are strong enough to stick them to a magnet or separate them from solution under an external magnetic field. It is also found that the maximum magnetic strength is not linear with the amount of Fe_3O_4 NPs. This phenomenon may be ascribed to multiple factors determining the magnetism of the Fe_3O_4@CMPs. The hybrid concentration of the Fe_3O_4 NP core, the thickness of the CMP shell and the size of the spacer may all have different levels of effects on the magnetic performance of the Fe_3O_4@CMPs. To

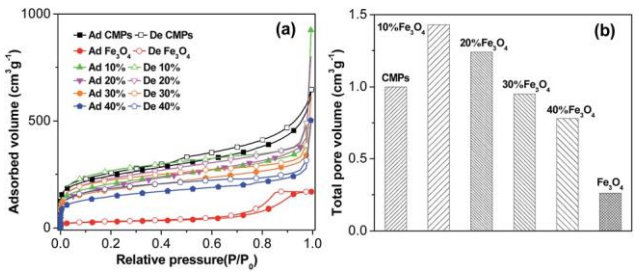

Fig. 2 (a) Nitrogen adsorption–desorption isotherms, and (b) total pore volume.

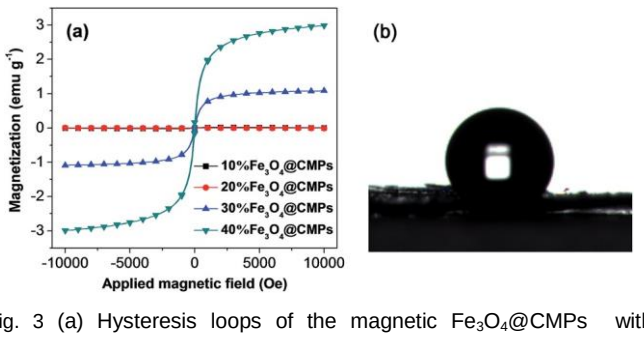

Fig. 3 (a) Hysteresis loops of the magnetic Fe_3O_4@CMPs with different Fe_3O_4 weight ratios, and (b) surface wettability test: an image of a drop of water on the 30% Fe_3O_4@CMP surface.

use this multifunctional hybrid material in complex application environments, its porous structure and magnetism had been shown above; surface wettability is another critical function. If the absorbent has strong hydrophobicity, it is easy to collect when treating the polluted water. The surface wettabilities of the Fe_3O_4@CMPs were studied (Fig. 3b). It was found that the contact angle is in the range of 114–124° for water, which demonstrates the hydrophobic nature of the hybrid materials. The highly hydrophobic surfaces plus the low density of the organic pores make the adsorbent keep 珠oating on the surface or the near surface region. The preliminary water system application test is shown in Fig. 4a–c. A hybrid polymer powder was added into an ampoule under ultrasound conditions until the powder was fully dispersed in the water, and then a block of magnet was waggled around the ampoule quickly, a泯er which the dispersed powder automatically formed into a ball and moved following the magnet. The hybrid powder was then collected from the water, and the ratio of the residue is about 97% a泯er ten times recycling. Crude oil polluted water as shown in Fig. 4d and 5 mg of hybrid powder were put onto the center of a Petri dish, and then a block of magnet was 珶xed on the le泯 side of the Petri dish. Five seconds later, the hybrid powder was automatically assembled onto the le泯 surface of the water, and the thickness of the crude oil layer showed an obvious reduction upon visual inspection (Fig. 4e). A泯er 15 s, most sections of the polluted surface turned clear and the permanent magnetic powder assembled together under the magnetic 珶eld (Fig. 4f). This result shows that the core@shell porous material is very suitable for crude oil treatment.

We also investigated the adsorption capacity of other organic solvents using the same method as reported[3b] (Fig. 4g and Table S2†). The adsorption capacity of the Fe_3O_4@CMPs ranges from 300 to 1600 wt%. They are excellent adsorbents for halogen solvents, such as chloroform and dichlorobenzene. It can be clearly seen that the adsorption capacity of the hybrid materials decreases as the Fe_3O_4 ratio increases from 10% to 40%, which may be explained by the fact that the hybrid materials with lower Fe_3O_4 concentrations possess higher total pore volumes and larger BET surface areas. As the kinetic diameters of the selected organic solvents are smaller than the pore size of the composite materials, the solvents can be adsorbed into the micro/mesopores and the space reservoir region of the core@shell formed by the etched $CaCO_3$. Therefore, the adsorption capacity may be in珠uenced by the density of solvents, total pore volumes and surface areas. In addition, their magnetic properties help them to be easily attracted and separated by applying an external magnetic 珶eld. Considering the superior adsorption capacity of organic solvents and unique magnetic properties, these materials have great potential for the removal of contaminants in water systems.

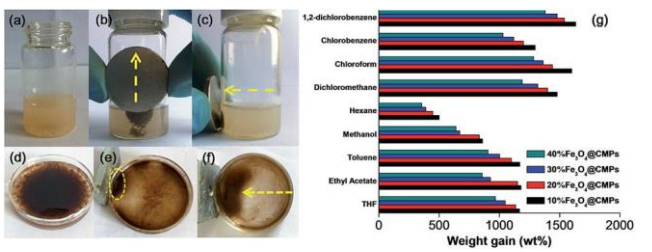

Fig. 4 Movement of the dispersive Fe_3O_4@CMPs in water under a magnetic field. (a) 10 mg of porous materials was added in 3 mL water under sonication until getting a homodisperse phase. (b and c) A block of magnet is moved upwards and to the left side around the ampoule. (d–f) Oil adsorption test. (d) Crude oil polluted water surface (10 cm diameter). (e) 5 mg of the Fe_3O_4@CMPs put onto the centre of the Petri dish after 5 seconds. (f) The porous materials automatically adsorbed the crude oil and assembled onto the water surface after 15 seconds. (g) Adsorption capacity of lab solvents.

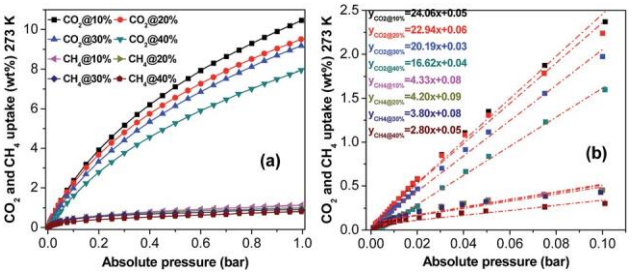

Fig. 5 (a) CO_2 and CH_4 adsorption isotherms at 273 K, and (b) fitting of the initial gas uptake slopes.

Methane is the main component of natural gas, is available in large quantities and has a high ratio of hydrogen/carbon compared to other hydrocarbons, but during CH_4 transportation, the existence of CO_2 reduces the energy density of natural gas and seriously corrodes the pipelines, especially in humid environments. The alkalescent nitrogen and ultramicropore containing polycarbazole shell can provide high sorption enthalpy for acidic CO_2 gas; meanwhile the magnetic core can 珶rmly 珶x the adsorbent in the separation 珽eld, avoiding the adsorbent loss as the CH_4 gas 珶ows. CO_2 and CH_4 isotherms of the hybrid materials were collected at 273 K as shown in Fig. 5a and S12.† The captured CO_2 is 10.47%, 9.51%, 9.18% and 7.95 wt% for 10–40% Fe_3O_4@CMPs, respectively, which are comparable with other reported organic porous polymers. The ideal gas CH_4/CO_2 selectivity estimated using the ratios of the Henry law constants calculated from the initial slopes of the isotherms in the low pressure range is shown in Fig. 5b. Linear 珶tting calculations show that the CO_2/CH_4 selectivity is 5.6, 5.4, 5.3 and 5.9, respectively. The four hybrid materials have a nearly similar selectivity, indicating that the microporous shell structure is the key to small molecular separation and the space between the shell and core provides a storage bin for the CO_2 adsorbate. In their practical application, optimization of the trade-off between the BET surface area, total pore volume and intensity of the magnetism needs to be done 珶rst.

Conclusions

In summary, we designed and synthesized polycarbazole based multifunctional hybrid materials Fe_3O_4@CMPs with a core–spacer–shell structure. Magnetism, a conjugated π-system and a porous structure are combined in one bulk material. These

materials can be used as dynamic adsorbing (water treatment) and static separation (gas CH_4/CO_2 selectivity) two working modes under magnetic field. The hydrophobic and low density properties enable those materials to adsorb pollutants from water with low cost, especially in dangerous environments. The intensive magnetism and ultramicroporosity are favourable for industrial (such as power stations) small molecular separation and avoiding raised dust produced by adsorbent loss. More work is needed to optimize the multifunctionality and trade-off the BET surface, pore width distribution, magnetism and wettability of these miraculous materials.

Acknowledgements

This work was supported by the National Natural Science Foundation of China (21274161 and 51573205), National "Twelfth Five-Year" Plan for Science and Technology Support (2015BAD16B05), and Scientific Research Project of Beijing Educational Committee (KM201410020011).

Notes and references

1 J.-X. Jiang, F. Su, A. Trewin, C. D. Wood, N. L. Campbell, H. Niu, C. Dickinson, A. Y. Ganin, M. J. Rosseinsky, Y. Z. Khimyak and A. I. Cooper, *Angew. Chem., Int. Ed.*, 2007, 46, 8574–8578.

2 (*a*) S. Qiao, Z. Du and R. Yang, *J. Mater. Chem. A*, 2014, 2, 1877–1885; (*b*) A. Li, H.-X. Sun, D.-Z. Tan, W.-J. Fan, S.-H. Wen, X.-J. Qing, G.-X. Li, S.-Y. Li and W.-Q. Deng, *Energy Environ. Sci.*, 2011, 4, 2062–2065; (*c*) S. Qiao, Z. Du, C. Yang, Y. Zhou, D. Zhu, J. Wang, X. Chen and R. Yang, *Polymer*, 2014, 55, 1177–1182.

3 (*a*) O. K. Farha, A. M. Spokoyny, B. G. Hauser, Y.-S. Bae, S. E. Brown, R. Q. Snurr, C. A. Mirkin and J. T. Hupp, *Chem. Mater.*, 2009, 21, 3033–3035; (*b*) A. I. Cooper, *Adv. Mater.*, 2009, 21, 1291–1295; (*c*) X. Chen, S. Qiao, Z. Du, Y. Zhou and R. Yang, *Macromol. Rapid Commun.*, 2013, 34, 1181–1185.

4 Y. Kou, Y. Xu, Z. Guo and D. Jiang, *Angew. Chem., Int. Ed.*, 2011, 50, 8753–8757.

5 (*a*) M. Rose, A. Notzon, M. Heitbaum, G. Nickerl, S. Paasch, E. Brunner, F. Glorius and S. Kaskel, *Chem. Commun.*, 2011, 47, 4814–4816; (*b*) K. Zhang, D. Kopetzki, P. H. Seeberger, M. Antonietti and F. Vilela, *Angew. Chem., Int. Ed.*, 2013, 52, 1432–1436.

6 X. Liu, Y. Xu and D. Jiang, *J. Am. Chem. Soc.*, 2012, 134, 8738–8741.

7 P. Robinson, P. Dunnill and M. Lilly, *Biotechnol. Bioeng.*, 1973, 15, 603–606.

8 X. Zhao, Y. Shi, T. Wang, Y. Cai and G. Jiang, *J. Chromatogr. A*, 2008, 1188, 140–147.

9 (*a*) C. Wang, J. Yan, X. Cui, D. Cong and H. Wang, *Colloids Surf., A*, 2010, 363, 71–77; (*b*) J. Zhou, W. Wu, D. Caruntu, M. Yu, A. Martin, J. Chen, C. O'Connor and W. J. Zhou, *J. Phys. Chem. C*, 2007, 111, 17473–17477.

10 X. Zhao, Y. Shi, Y. Cai and S. Mou, *Environ. Sci. Technol.*, 2008, 42, 1201–1206.

11 S. Wang, H. Niu, T. Zeng, X. Ma, Y. Cai and X. Zhao, *CrystEngComm*, 2014, 16, 5598–5607.

12 Z. Liu, H. Wang, C. Liu, Y. Jiang, G. Yu, X. Mu and X. Wang, *Chem. Commun.*, 2012, 48, 7350–7352.

13 (*a*) X. Yang, B. Li, I. Majeed, L. Liang, X. Long and B. Tan, *Polym. Chem.*, 2013, 4, 1425–1429; (*b*) Q. Gao, C. Lin, D. Luo, L. Suo, J. Chen and Y. Feng, *J. Sep. Sci.*, 2011, 34, 3083–3091.

14 W. Zhang, F. Liang, C. Li, L. Qiu, Y. Yuan, F. Peng, X. Jiang, A. Xie, Y. Shen and J. Zhu, *J. Hazard. Mater.*, 2011, 186, 984–990.

15 (*a*) C. Zhao, W. Wang, Z. Yu, H. Zhang, A. Wang and Y. Yang, *J. Mater. Chem.*, 2010, 20, 976–980; (*b*) A. Olejniczak, M. Lezanska, J. Wloch, A. Kucinska and J. P. Lukaszewicz, *J. Mater. Chem. A*, 2013, 1, 8961–8967.

16 (*a*) Q. Chen, M. Luo, P. Hammershøj, D. Zhou, Y. Han, B. W. Laursen, C. Yan and B. Han, *J. Am. Chem. Soc.*, 2012, 134, 6084–6087; (*b*) S. Qiao, Z. Du and R. Yang, *J. Mater. Chem. A*, 2014, 2, 1877–1885; (*c*) Y. Zhang, A. Sigen, Y. Zou, X. Luo, Z. Li, H. Xia, X. Liu and Y. Mu, *J. Mater. Chem. A*, 2014, 2, 13422–13430; (*d*) J. Gai, X. Gong, W. Wang, X. Zhang and W. Kang, *J. Mater. Chem. A*, 2014, 2, 4023–4028.

17 T. Kuo, C. Weng, C. Chen, Y. Chen, C. Chang and J. M. Yeh, *Polym. Compos.*, 2012, 33, 275.

18 K. I. Kim, C. Basavaraja and D. S. Huh, *Bull. Korean Chem. Soc.*, 2013, 34, 1391–1396.

19 H.-X. Wu, X.-Q. Qiu, R.-F. Cai and S.-X. Qian, *Appl. Surf. Sci.*, 2007, 253, 5122–5128.

20 Q. Zhang, Y. Yang and S. Zhang, *Chem.–Eur. J.*, 2013, 19, 10024–10029.

21 K. S. Sing, D. H. Everett, L. Moscou, R. Pierrotti, J. Roquerol and T. Siemeniewska, *Pure Appl. Chem.*, 1985, 57, 603–619.

22 (*a*) J. Weber, J. Schmidt, A. Thomas and W. Böhlmann, *Langmuir*, 2010, 26, 15650–15656; (*b*) Y. Zhu, H. Long and W. Zhang, *Chem. Mater.*, 2013, 25, 1630–1635.